ELSEVIER

Biophysical Chemistry 66 (1997) 211–228

Biophysical Chemistry

Kinetic Investigations by Fluorescence Correlation Spectroscopy: The Analytical and Diagnostic Potential of Diffusion Studies

Petra Schwille*, Jan Bieschke, Frank Oehlenschläger§

Max-Planck-Institut für Biophysikalische Chemie, Abteilung Biochemische Kinetik, D-37077 Göttingen, Germany
§ Present address: EVOTEC BioSystems GmbH, D-22529 Hamburg, Germany

Received 24 April 1997; accepted 24 April 1997

Abstract

This review demonstrates the large analytical and diagnostic potential of fluorescence correlation spectroscopy applied to freely diffusing biomolecules in solution. All applications discussed here in detail are based on changes in the diffusion characteristics of fluorescenctly labeled complementary strands of nucleic acids when they associate. However, the principle of the measurement can be extended to many different reactions with characteristic association times between several minutes up to several hours. If the reaction significantly affects the diffusion constants of at least one partner, single-color autocorrelation analysis is sufficient to extract kinetic parameters. If the observed binding process has only a moderate effect on diffusion coefficients, the detection selectivity and sensitivity can be improved by dual-color cross-correlation analysis. Finally, we show that diffusional analysis on the single-molecule level even opens up diagnostic applications, such as the detection of minute amounts of infectious agents like HIV-1 viruses in blood. © 1997 Published by Elsevier Science B.V.

Keywords: Number fluctuation; Confocal optics; Single molecule detection; Cross-correlation; RNA; DNA; Renaturation; Hybridization; HIV-1; NASBA

1. Introduction

1.1. Principles and applications of fluorescence correlation spectroscopy (FCS)

In contrast to conventional applications of fluorescence spectroscopy where the emission from comparatively large ensembles of fluorescent molecules is collected and analyzed, fluorescence correlation spectroscopy mainly focuses on the small statistical fluctuations of this signal. The idea for investigating these minute deviations in their dynamics is based on the assumption that the phenomenological laws describing the relaxation of a macroscopic system to equilibrium following a perturbation hold also for spontaneous microscopic events [1,2]. Hence, by

PII S0301-4622(97) 00061-6

resolving and temporally analyzing fluctuations, the dynamics of macroscopic processes may be investigated without perturbing the equilibrium state.

Fluorescence is a highly specific and sensitive parameter for detecting fluctuations on the scale of individual molecules, and fluorescence fluctuation analysis has opened up new perspectives in physical chemistry. Although several possibilities exist for relating molecular dynamics of fluorescent particles to variations in fluorescence light intensity, one remarkably simple and popular method is the investigation of number fluctuations in an open detection volume element; this is the so-called concentration correlation spectroscopy [3].

Number fluctuation may be mediated by different processes, such as particle movement, chemical reactions or aggregation. Early theoretical descriptions of number fluctuations of mobile particles in a fixed, open volume element [4,5] were exploited in the development of quasi-elastic light scattering [6]; these concepts were 1972 applied by Magde *et al.* [7] by employing fluorescence correlation spectroscopy (FCS) which extended fluctuation analysis to a broader area of biophysical problems. In the following years, comprehensive theoretical concepts and several experimental proofs for following translational and rotational diffusion, reversible isomerisation and bimolecular chemical reactions were published [8,9,10,11,12].

Autocorrelation analysis is performed by multiplying the spontaneous fluctuations of the fluorescence intensity with themselves at different delay times τ, and averaging this product in a statistical manner for a large number of single fluctuation events. This autocorrelation curve decays from a maximum value at $\tau = 0$ to zero for large delay times τ. Because the magnitude of the fluctuations is directly related to the average number of fluorescent particles in an observed volume element, obeying Poissonian statistics for low particle numbers, the amplitude of the normalized fluctuation correlation curve ($\tau = 0$ value) is inversely proportional to this average occupation number, so that it is a sensitive tool for measuring concentrations. Beyond that, it has already been used for determining molecular weights of DNA [13] and aggregation of particles in ideal and nonideal solutions and on surfaces [14,15,16,17]. For these special purposes, theoretical and experimental concepts of higher order correlation [18] and scanning- (later imaging-) FCS have been developed [19,20,21,22,23].

On the other hand, the temporal decay of the correlation function for delay times $\tau > 0$ provides information on the dynamic behavior of the system and can be regarded as a relaxation curve of the statistical deviations from equilibrium. In purely diffusive systems where no additional molecular effects are present, the decay rate of the correlation simply reflects the diffusion of the fluorescent molecules out of the illuminated detection volume; therefore it is a means for analyzing diffusion characteristics. A wide variety of FCS diffusion measurements in solutions and on natural and artificial membranes has been reported [24,25,26,27,28,16]. General concepts for quantifying nondiffusional translocation of the sample, such as laminar flow, have also been provided [29,30]. Cross-correlation schemes were developed for measuring pairwise particle interactions [31] and for determining the direction of flow in sample streams [32,33].

1.2. Confocal FCS and single-molecule detection

With the availability of powerful laser sources with high spatial and temporal coherencies and ultrasensitive photocounting devices, extremely small volume elements can be investigated. Our work is based on the confocal application of fluorescence correlation spectroscopy following the work of Rigler *et al.* [34,35,36] where the resolution has been extended such that the temporal behavior of single molecules can be followed. Here, an extremely small measurement volume of less than 10^{-15}l is defined by a microscope objective with high numerical aperture which is epi-illuminated by a laser beam; the fluorescence light from the so defined focal volume in a sample is imaged onto the detector surface. By using concentrations of fluorescent particles in the nM range, the temporal average of the number of contemporary detected molecules can be reduced to 1 or even below. Using an additional two-detector device with temporal resolution which allows extremely short correlation times, it was possible for Widengren *et al.* [37,38] to investigate the relaxation time con-

stants of intersystem crossing of a dye into its triplet state during the diffusion measurements in this confocal setup. Having reached the single-molecule detection level, a wide variety of further investigations are opened up [39], among them as ambitious projects as single-molecule DNA sequencing (see the review of Brinkmeier *et al.* in this issue) and the diagnosis of single infectious particles in blood or serum, that is one of the topics of this review. However, in contrast to methods where individual single molecules are traced, the applications described here are based on the statistical behavior of freely diffusing particles in large thermodynamic ensembles, where correlation analysis is necessary to obtain adequate information about the system. It can be shown that by simply determining the average molecular diffusion properties, many kinetic applications, such as nucleic acid hybridization, receptor-ligand interaction, and even viral diagnostics become feasible. Here we focus on work that has been carried out in our group based on specific hybridization and renaturation reactions of labeled DNA probes to RNA and DNA target molecules.

2. Kinetic studies and FCS applications

A central aspect of biophysical chemistry is the determination of reaction kinetics of biological systems, and there are numerous studies on this subject. A variety of methods have been developed for measuring ultrafast processes on one hand and for detecting minute amounts of material on the other hand. Rapid flow, relaxation and NMR methods are prominent examples of the first category [40,41] while techniques based on labeling the reaction partners with radioactive or fluorescent probes fall into the second. The biochemical reaction that is probably the most fundamental of all in biology is the base-pairing reaction between nucleic acids. By this reaction, an ensemble of positive and negative strands of nucleic acids has the inherent property of self-replication which is understood to underlie all evolutionary processes [42,43]. Nucleic acid hybridization is the primary means for the propagation of information in replication, transcription and translation. First, a short synopsis of other techniques used for studying nucleic acid hybridization shall be given.

2.1. Techniques in hybridization and renaturation kinetics

In order to follow the time course of base-pair formation, one has to monitor the concentration of the single-stranded and double-stranded species separately. To achieve this goal, techniques for studying hybridization kinetics can be divided roughly into two categories: first, methods in which the components are physically separated prior to detection, and second, methods that monitor the components of the reaction directly in solution. Whereas, in general, the first approach is more sensitive and is superior for detecting small quantities of nucleotides, artifacts due to interactions with the solid phase cannot be ruled out completely, and the accuracy of quantitation depends on the detection system.

Separation techniques: Filter binding assays were used by Britten and Kohne in their classical analysis of nucleic acid hybridization for studying gene complexity and gene copy number [44,45]. The assay employs single-stranded DNA immobilized on a nitrocellulose filter or a similar support. The filter is incubated with labeled RNA probes and the unhybridized probes are rinsed off after incubation. This technique has been standardized to a great extent and finds widespread use as 'Southern blotting' and related methods in viral diagnostics. While it provides an easy and rapid way of measuring the amount of nucleic acid present in a probe, the reaction conditions of this method are not well characterized and consequently the kinetic parameters differ from those obtained in solution [46]. To detect the hybridized product sensitively, the oligonucleotide probe has to be labeled. This is classically done by incorporating radioactively labeled nucleotides, i.e. ^{32}P or ^{111}In, which can be detected by autoradiography. More recent forms of labeling, reviewed by Wetmur [47], avoid the inconveniences of radionucleotides by using fluorescence labeling or indirect labeling techniques. Most frequently, a biotin label is attached to the oligonucleotide which can be linked to a reporter system. Enzymatic reporter systems which catalyze a colorimetric reaction have detection thresholds of picograms [48]. Recently, Watts *et al.* [49] directly

monitored DNA-DNA hybridization using oligonucleotide probes immobilized on optical biosensors. The binding of the target oligonucleotide in the nanomolar range could be detected quantitatively.

In other separation techniques the hybridization of the target sequence with the labeled probe is carried out in solution, thereby avoiding interactions with the solid phase. The hybridized product is subsequently separated from the reactants. Single-stranded and double-stranded nucleotides can be separated on a hydroxyapatite column [50]. Nuclease resistance can also be used to monitor the hybridization reaction if the hybridized nucleotide strands are challenged by a single-strand-specific nuclease. Hybridized radioactively labeled probes have been incubated with Nuclease S1 [51] or RNase H [52]; the amount of remaining double stranded polynucleotides was then determined by precipitation. Kumazawa *et al.* [53] have used non-denaturing gel electrophoresis for the separation of hybridized from non-hybridized nucleotides; chromatographic methods (HPLC) have been employed by Dewanjee *et al.* [54] for the hybridization of mRNA with ^{111}In-labeled oligo-DNA. Due to its great resolving power, capillary gel electrophoresis (CGE) has become an effective tool for separating hybridized and nonhybridized nucleic acids [55]. It can be combined with absorption spectroscopy [56], fluorescence detection [57] and mass spectrometry [58] to quantify the amount of nucleic acids.

Solution measurements: A more straightforward approach is the monitoring of paired and unpaired nucleotides directly in solution. In the past this has been achieved by absorption spectroscopy using the decrease of absorption (hypochromicity) or the change in circular dichroism [59] of the nucleotides on forming base-paired helices. The cooperative mechanism of the helix-coil transition of oligonucleotides has been elucidated by stopped-flow and relaxation measurements using absorption spectroscopy [60]. Calorimetry [61] and nuclear magnetic resonance [62] are also suited for solution hybridization studies. These techniques all require μg-mg amounts of nucleic acids, which often are not easily available.

Recently, sensitive fluorescence measurements have been used to directly monitor the hybridization of nucleotides in solution. One approach utilizes the quenching of certain fluorophores like pyrene when binding to a double-stranded nucleic acid chain. Li *et al.* [63] determined the association and dissociation rates of a pyrene-labeled 4-mer to the L-21 *Sca* I ribozyme as a function of temperature and thereby calculated the activation enthalpy for the binding process. The fluorescence detection was coupled to a stopped-flow apparatus. The technique also requires rather large samples in the range of μg-mg.

An interesting variation on the theme of fluorescence quenching involves the molecular beacons used by Tyagi and Kramer [64] to monitor nucleic acid synthesis. They developed a DNA probe which folds back on itself into a hairpin structure, where the fluorophore attached to one end of the oligonucleotide is brought next to a quencher molecule located at the other end of the nucleic acid strand. The fluorophore emits light only when the probe is hybridized to a target nucleic acid sequence. In another approach [65] a DNA oligomer was labeled with a donor fluorescent dye at the 3'-end and with an acceptor dye at the 5'-end. Due to the strong dependence of energy transfer efficiency on the distance between the donor and the acceptor dye, the emission spectra of the free and the hybridized probes are strikingly different. This fact was exploited to determine the kinetics of duplex formation. Fluorescence resonance energy transfer (FRET) was also employed to study the binding of the labeled oligomer to a M13 single stranded DNA target. Labeling of one oligonucleotide strand with a donor and the other with an acceptor dye has been used by Perkins *et al.* [66] in the analysis of ribozyme-binding kinetics.

2.2. *Possibilities to use FCS in kinetic studies*

Fluorescence correlation spectroscopy, in its confocal form, provides sufficient sensitivity, so that the photon bursts of single molecules are detected. The measurements are applicable over a wide time range, which is useful for kinetic measurements. Determination of chemical reaction rates by fluorescence correlation analysis was originally provided for systems where reversible chemical reactions cause significant fluctuations in fluorescence light emission, such as the binding of ethidium bromide to DNA

[7,10]. This reaction scheme has found several applications [67,68]; it presumes that the chemical relaxation time is fast compared to the residence time of interacting particles in the observation volume, thereby allowing the contributions of diffusion and reaction to be mathematically separated in the correlation curve. Another possibility for quantifying reaction rates of fluorescent molecules is found in systems where the molecular association results in dramatic changes of the diffusion characteristics of the fluorescent partner; in extreme cases this can lead to complete immobilization [69].

Unlike reaction schemes where fluctuations in the extent of reversible chemical binding take place, the application of FCS to kinetic systems reported in this article is based on the highly specific, irreversible binding of fluorescently labeled molecules to larger partners that results in immediate slowing down of the diffusion. In such cases, the time-dependent changes of diffusion constants extracted from the correlation curve provides an indirect measure for the ongoing reaction.

The high sensitivity of confocal FCS to changes in diffusion characteristics of the observed fluorophores, for example, made it possible for Kinjo and Rigler [70] to follow the irreversible binding of a fluorescently labeled 18mer DNA primer at a concentration of 50 nM to a 7.5 kb DNA containing the complementary sequence. It has been shown by Rauer *et al.* [71] that this kind of FCS analysis is by no means restricted to nucleic acid interactions. In their study the interaction kinetics of tetramethylrhodamine-labeled a-bungarotoxin with the nicotinic acetylcholine receptor (AChR) of the torpedo fish was determined by utilizing the considerable increase of the diffusion coefficient of the toxin when binding to the 290000 kD AChR-1 monomer. The results show that FCS diffusional analysis, due to its extreme sensitivity, is optimally suited for following highly specific but comparatively slow reactions (minutes to hours) with high association and low dissociation rates in physiological concentration ranges; this indicates the applicability of FCS for drug screening and diagnostics. Recently, competition assays of EGF-receptor systems and enzymatic digestion studies using FCS were reported [72]. In principle, measurements can be performed in any optically transparent liquid environment without the necessity of educt-product separation.

The experiments of Magde *et al.* [7] and the investigations reported here which follow the concept of Kinjo and Rigler [70] display the two time ranges in which kinetic processes can be evaluated by FCS. First, processes that occur fast compared to the average diffusion time enter directly into the correlation function. Second, processes in the time range of minutes to hours can be monitored by consecutive FCS diffusion analyses, giving a quasi-static picture of the state of the reaction at any time.

3. Performing and evaluating diffusion measurements

3.1. Experimental setup and fluorescent probes

Figure 1 shows a schematic view of our confocal FCS experimental setup. Parallel laser light fills the back aperture of a Zeiss infinity-corrected microscope objective with a high numerical aperture (Plan Neofluar 40×0.9 or Plan Neofluar 63×1.2); the light is focused at an angle δ. This angle depends on the cross-section of the illuminating beam and defines the lateral dimension of our effective measurement volume [73].

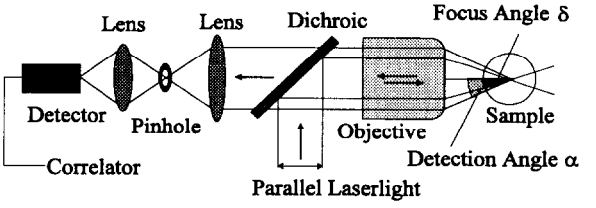

Fig. 1: Confocal FCS setup. Fluorescence is excited by focussing parallel laserlight by the objective at an angle δ, detection is performed through the same objective at an angle α. The detector signal is temporally autocorrelated.

Fluorescence arising from the illuminated cone is collected by the same objective and passes a dichroic mirror; the observed solid angle is given by the numerical aperture and should be as large as possible. A pinhole in the image space allows light emanating from different depths to be discriminated and defines the axial dimension of the detection volume. The so

obtained three-dimensional focal spot is then imaged onto the surface of the highly sensitive avalanche diode (EG&G SPCM-200). The diode signal is correlated quasi on-line with a digital PC correlator board (ALV-5000), this comfortably allows us to follow the correlation curve in real time on the PC monitor. The solution under the objective contains the biochemical reaction system in a chosen buffer. The sample can simply be suspended as a droplet under the objective lens or, as in our case, it may be contained in a specially designed thermostatted sample carrier. As described below, sealable reaction vessels are preferable for diagnostic purposes.

To achieve adequate detection specificity and sensitivity, most bioactive molecules must be fluorescently tagged, either by intercalating nucleic acid stains or by covalently linking single fluorophores, the latter is usually more suitable. The dye tetramethylrhodamine used in all single-color applications is linked to the nucleic acid molecules by an aminohexyl linker and exhibits a high quantum yield and a high photostability. It has been shown by Koppel [74] that the signal-to-noise ratio (S/N), and thereby the sensitivity of the method, is given by the average photon-count rate per detected molecule. In confocal FCS applications, S/N values of up to 1000 have been achieved [36,75]. Count rates of several 10.000 photocounts per second per molecule are easily obtained with rhodamine dyes, in our setup. Photobleaching is minimized by the short residence times of the dye in the confocal volume element. Dichroic mirrors and proper filter sets, as well as very small pinholes guarantee that only the fluorescence light emanating from a focal region of less than 10^{-15}l can be detected. For concentrations in the range of nM or below, one can thus be sure that the measured fluctuations arise from the dynamics of single fluorescent molecules. In the simplest case these fluctuations are caused by molecules diffusing through the illuminated region, being fluorescent only during this restricted time interval. The duration of a so obtained fluctuation depends in a fixed optical setup directly on the velocity of the molecule and on its path through the illuminated region. For data collection times that are long compared to the average residence time of the molecules in the detection volume, a large number of single diffusion events can be analyzed and an average diffusion time can be determined for any molecular species. Data collection times are typically 30-120 s in our applications. When the average diffusion times of the observed molecules are in the ms time range, thousands of single diffusion events contribute to the correlation curves, giving them a high statistical accuracy.

3.2. *Theoretical concept of diffusion studies*

The normalized fluctuation autocorrelation function G(τ) for a fluorescence intensity signal F(t) fluctuating around a temporal average

$$F(t) = \langle F(t) \rangle + \delta F(t) \tag{1}$$

is for any delay time τ given by

$$G(\tau) = \langle \delta F(t) \delta F(t+\tau) \rangle \Big/ \langle F(t) \rangle^2 . \tag{2}$$

The brackets denote temporal averages, and δ is the fluctuation symbol. The fluorescence intensity from an illuminated sample can be regarded as the integral product of fluorescent particle concentration C(r,t) and the space-dependent intensity of the fluorescence light emission E(r) [76]. This emission intensity again is a complex product of excitation light intensity, the quantum yield of the fluorophore, filter and detector efficiency and the characteristic spatial transfer function under which the optical system (consisting of the objective and a pinhole) collects light, the so-called "collection efficiency function" [73], that shall no further be regarded here.

The integration $F(t) = \int E(\underline{r}) C(\underline{r}, t) dV$ is carried out to infinity over the whole space V, and the autocorrelation function Eq. 2 becomes

$$G(\tau) = \frac{\int\int E(\underline{r}) E(\underline{r}') \langle \delta C(\underline{r},0) \delta C(\underline{r}', \tau) \rangle dV dV'}{\left(\langle C \rangle \int E(\underline{r}) dV \right)^2} . \tag{3}$$

In this expression, it can easily be seen that the temporal information is exclusively determined by the thermodynamic concentration fluctuations or rather, by fluctuations in the molecular number density at any spacepoint r. These fluctuations are medi-

ated by the random Brownian motion of the particles, so that the obtained Gaussian expression for the concentration correlation term in the numerator of Eq. 3 becomes in three dimensions for a species with diffusion coefficient D [8,77]:

$$\langle \delta C(\underline{r},0)\delta C(\underline{r}',\tau)\rangle = \langle C\rangle(4\pi D\tau)^{-3/2}\exp\left(-(\underline{r}-\underline{r}')^2/4D\tau\right) \quad (4)$$

This expression is closely related to the general solution of the diffusion equation which describes the transition probability for a particle from $\underline{r}$ at time 0 to $\underline{r}'$ at time τ [78].

One can easily prove that the convolution of the concentration correlation term Eq. 4 with a Gaussian-distributed emission light intensity $E(\underline{r})$ with $1/e^2$-distances r_0 and z_0 for the lateral and axial Gaussians respectively, results in an analytical solution for the fluorescence autocorrelation function of freely diffusing fluorophors. For two-dimensional geometries or infinite extension in the z-direction ($z_0 \rightarrow \infty$) it reads [8]:

$$G(\tau) = G(0)\cdot\left(1+\tau/\tau_d\right)^{-1}. \quad (5a)$$

τ_d is related inversely to the diffusion coefficient: $\tau_d = r_0^2/4D$, and equals the time $\tau_{1/2}$ when $G(\tau)$ dropped to one half: $G(\tau_{1/2}) = G(0)/2$. In the three-dimensional case or restricted z-extension, $G(\tau)$ is described by [12,34]:

$$G(\tau) = G(0)\cdot\left(1+\tau/\tau_d\right)^{-1}\cdot\left(1+r_0^2\tau/z_0^2\tau_d\right)^{-1/2} \quad (5b)$$

In order to better compare with the two-dimensional situation, the characteristic decay time τ_d in both, Eq. 5a and 5b, denotes the average time a molecule needs for diffusing out of this volume in a lateral direction, once it is detected. It can be shown that both analytical approximations (5a) and (5b) are feasible with a proper choice of the pinhole [79,73]. For three-dimensional geometries with larger values $z_0 > 3\ r_0$, like in our case, τ_d approximately equals the characteristic half-value decay time $\tau_{1/2}$. The amplitude G(0) is inversely proportional to an effective detection volume V_{eff} [76] and to the particle concentration C: $G(0) = V_{eff}^{-1}\langle C\rangle^{-1}$.

In diffusion systems with more than one fluorescent species i, when the molecules are indistinguishable by their fluorescence characteristics, the overall autocorrelation decay time $\tau_{1/2}$ is composed of several single contributions τ_i. The fluorescence correlation function is then a simple sum of individual contributions of the separate components:

$$G_{tot} = \sum_{i=1}^{M}\langle C_i\rangle Diff_i \Big/ V_{eff}\left(\sum_{i=1}^{M}\langle C_i\rangle\right)^2 = N_{tot}^{-1}\sum_{i=1}^{M} Y_i Diff_i \quad . \quad (6)$$

Eq. 6 is written for M different species, where

$$Diff_i \equiv \left(1+\tau/\tau_i\right)^{-1}\left(1+r_0^2\tau/z_0^2\tau_i\right)^{-1/2}$$

is an abbreviation for the contribution of the independently diffusing different species i with lateral diffusion times $\tau_i = r_0^2/4D_i$ to the temporal decay of G_{tot}, and Y_i is their relative fraction:

$$Y_i = \langle C_i\rangle \Big/ \sum_{i=1}^{M}\langle C_i\rangle .$$

The total number of detected molecules in the effective volume element is given by

$$N_{tot} = V_{eff}\sum_{i=1}^{M}\langle C_i\rangle .$$

When a small labeled probe reacts with a large unlabeled target molecule without affecting the fluorescence characteristics of the dye, the rates of diffusion are changed; this results in an increase in particle diffusion time τ_d and thereby in the overall correlation decay time $\tau_{1/2}$. In the ideal case, for a two-component system Eq. 6 reduces to

$$G_{tot} = N_{tot}^{-1}\left[(1-Y(t))Diff_1 + Y(t)\cdot Diff_2\right] , \quad (7)$$

with average diffusion times τ_1 in $Diff_1$ for the free probe and τ_2 in $Diff_2$ for the probe-target complex. If Y(t) denotes the fraction of bound probe molecules at any time in the reaction, the kinetics of irreversible binding is reflected by an increase of fraction Y from 0 at the beginning of the reaction to a stationary value less than or equal to 1 that is determined by the initial concentrations of the reactants. With the analytical expression Eq. 7, the total correlation function G_{tot} can be mathematically separated into the single contributions $Diff_1$ and $Diff_2$ at any time t, fitting the measured curves G_{tot} with a Marquardt nonlinear least-square routine. If this is done for consecutive measurements in the time course of hybridization, the plot of Y against time yields a kinetic curve that can be easily evaluated to obtain the association rate constants. Figure 2a shows a plot of typical correlation curves with the same values of N_{tot}, τ_1 and τ_2, but varying Y in a logarithmic time scale. If τ_1 and τ_2 differ by at least one order of magnitude, a two-step decay curve is obtained. If not, increasing values of Y are simply represented by a shift of the curves towards longer overall decay times $\tau_{1/2}$.

3.3. Evaluation and graphic representation of single-color measurements

To obtain kinetic data, the measured autocorrelation decay time $\tau_{1/2}$ must be decomposed into the single diffusion time contributions τ_i, as well as their fractions Y_i. Although mathematical evaluation by fitting routines is necessary for a correct quantitative analysis of the system, several rather simple approaches can be made to obtain a good estimate of the progress of reaction. In our instrument setups, the effective illuminated volume elements are approximately five times longer in z_0 than in r_0, with a quasi-Gaussian distribution of laser light in all directions. Hence, for small values of τ, the decay in Eq. 5b can be approximated to be hyperbolic (two-dimensional case). A very easy way to visualize differences in the overall decay time $\tau_{1/2}$ for cases where the difference between τ_1 and τ_2 is not too crucial ($\tau_2 < 5\tau_1$), is to plot G^{-1} against the linear time scale [80].

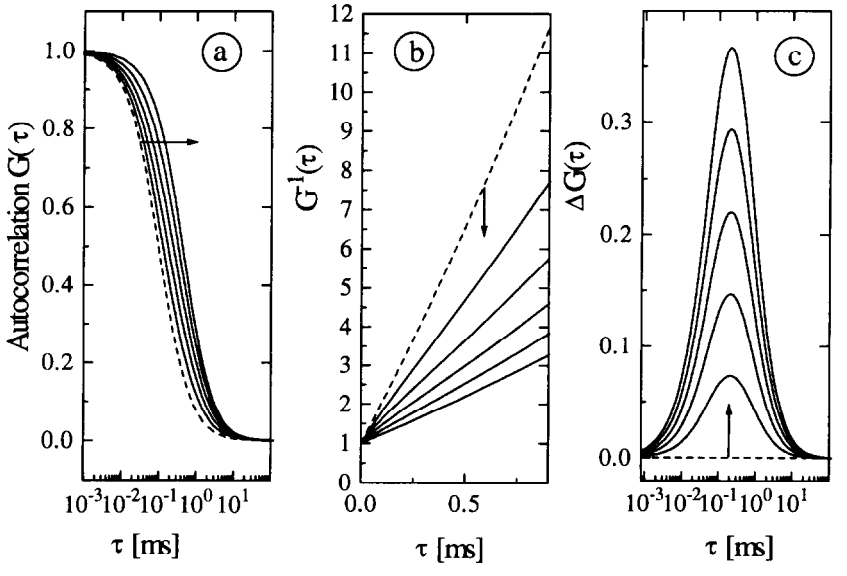

Fig. 2: Calculated autocorrelation curves for a two-component diffusion system (Eq. 7) with $\tau_1 = 0.1$ ms and $\tau_2 = 0.5$ ms, and increasing fractions Y (dashed line Y = 0, in arrow direction Y = 0.2, 0.4, 0.6, 0.8, 1) a) $G_{tot}(\tau)$ on logarithmic time scale, b) reciprocal on linear scale. For increasing fractions Y of slower species, the average decay time increases and the slope of the reciprocal drops. c) Difference curves, obtained by subtracting the Y=0 curve from the others as described in the text. The location of the maximum remains constant due to constant values τ_1 and τ_2, the amplitude is proportional to Y.

For any given concentration, the slope of the curve is then directly proportional to $\tau_{1/2}$, which is composed of τ_1 and τ_2. In Figure 2b, the correlation curves from Fig. 2a with an increasing value Y resulting in increasing decay times $\tau_{1/2}$ are represented in such a "reciprocal plot". Temporal changes of $\tau_{1/2}$ due to higher fractions of τ_2 can directly be followed during the reaction and allow for a good estimation of the reaction's progress.

By this rather simple graphic representation, one cannot decompose the correlation half-value decay time $\tau_{1/2}$ into the single diffusion time constants and fractions of the two species. A given shift in the autocorrelation decay time due to binding to larger molecules may result either from a large fraction Y of comparatively small τ_2 , or from a small fraction of an extremely slow product. For this reason, it is always necessary to determine as many parameters as possible in accurate calibration measurements. The best evaluation of Y(t) would be made if both, τ_1 and τ_2 were known in advance. For the above reaction schemes using a singly-labeled partner, at least the diffusion time of this partner (in our case free probe) can easily be determined. If there is no possibility to determine diffusion time τ_2 of the isolated probe-target complex in calibration measurements, an estimate of it can be given from the measured curves during the association as follows (for the sake of simplicity, the two-dimensional expression for temporal decay is used). The correlation curve of the labeled partner before an association takes place is given by:

$$G_1(\tau) = N_{tot}^{-1} \cdot \left(1+\tau/\tau_1\right)^{-1}; \tag{8}$$

for later times t, after the reaction has already progressed, and $Y \neq 0$, we obtain:

$$G_{1,2}(\tau) = N_{tot}^{-1} \cdot \begin{bmatrix} (1-Y)\left(1+\tau/\tau_1\right)^{-1} \\ +Y\left(1+\tau/\tau_2\right)^{-1} \end{bmatrix}. \tag{9}$$

Because the total number of measured fluorescent molecules N_{tot} is ideally not affected by the reaction, we can easily subtract Eq. 8 from Eq. 9. By differentiating the result with respect to τ, it can be shown, that the obtained difference curve has a maximum value when $\tau_m=(\tau_1\tau_2)^{1/2}$. This position on the τ-axis is only dependent on the diffusion times, not on the fractions Y; however, the maximal height is directly proportional to Y for given τ_1, τ_2. In ideal reaction schemes with time-independent diffusion characteristics of educt and product species, the amplitude of the maximum should increase without a change in its position on the τ-axis. Fig. 2c shows a theoretical example of this. Although this analysis cannot substitute evaluation by fitting routines, it is a good check whether the measurement parameters behave as expected. A significant shift in the difference curve ($G_{1,2}$-G_1) towards higher or lower τ_m during the reaction can always be an indication of non-idealities in the experiment, such as particle aggregation, the presence of fluorescent contaminants, or a photophysical degradation of the marker fluorophore.

As explained above, single-color fluorescence analysis of multicomponent diffusional systems, although very easy to perform, has two significant drawbacks. The first is the need of mathematically decomposing the "mixture" curves G_{tot} (Eq. 7) into the different decay time contributions from the free and bound reaction partners. It would be more attractive to plot a parameter measured directly during its temporal evolution; then the kinetic rate constants could also be derived directly rather than obtained by employing fitting routines.

The second shortcoming is much more crucial; this concerns the classes of reaction processes where free and bound partners can be discriminated by means of diffusional analysis at all. According to the Stokes-Einstein relation, the diffusion coefficient is inversely proportional to the hydrodynamic radius of the particles and thereby in first approximation to the third root of molecular weight. Hence, there will be no significant changes on the correlation curve during the association process for a considerably large class of bimolecular reactions of biomolecules. Recently, it has been shown that these problems can be prevented by means of dual-color crosscorrelation setups [76]. The last part of this theoretical section should therefore be concerned with this new extension of the FCS method.

3.4. The concept of dual-color cross-correlation

As pointed out, a shift in the correlation curves to longer decay times corresponds to a slowing down of molecular diffusion; this happens during the time course of reactions where a labeled probe binds to a much larger target molecule. On the other hand, the amplitude of the correlation curve is not sensitive to the reaction unless the number of fluorescent particles in the volume element changes. In the usual scenario, when the labeled reaction partner has a definite concentration, and binding to the target does not affect the fluorescence characteristics, the amplitude should remain constant in time and therefore cannot be used to evaluate reaction rate constants. However, there exists a possibility to follow dynamic processes by a change in the amplitude. This can be achieved in dual-color cross-correlation schemes: Here, both reaction partners are labeled with different dyes, so that in case of reaction a new fluorescent species arises, which is labeled by two dyes; this species can be followed by cross-correlating the two different emission signals. A great advantage of this application in respect to the single-color case, where the reaction is mapped by a change in diffusion time, is that in a proper setup the amplitude of the cross-correlation function is directly proportional to the concentration of the reaction product; therefore, kinetic information can be easily extracted from this parameter. No mathematical decomposition of a measured curve in contributions of free and bound educts is necessary. The second advantage is that the sensitivity of this method does not depend on the changes in molecular weight, which can be rather small if molecules of comparable size and structure are investigated. Here, a yes-or-no decision whether a reaction occured or not can be made by exclusively "scouting" for doubly-labeled molecules.

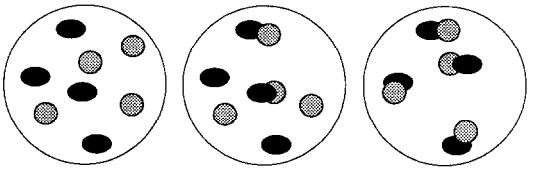

Fig. 3: Schematic for the principle of cual-color cross-correlation analysis. The two colors represent the different fluorescent species. From left to right: temporal evolution of an association reaction. The concentration of doubly-labeled species, represented by the amplitude of the cross-correlation curve, increases in time.

Fig. 3 gives a sketch of how the principle works. Two differently labeled molecules, e.g. green G and red R, irreversibly react to form a species GR bearing both dye labels, and the concentration of GR increases with time. The fluorescence emission from the system is split into two channels and detected by two wavelength-selective devices.

From the green and the red detector signals three correlation curves can be derived: green and red autocorrelation curves, as well as a green-red cross-correlation curve. The theoretical description for the three curves in an ideal dual-color system is given for any time during the reaction by [76]:

$$
\begin{aligned}
G_G(\tau) &= \left(\langle C_G\rangle Diff_G + \langle C_{GR}\rangle Diff_{GR}\right) \Big/ \left(V_{eff}\left[\langle C_G\rangle + \langle C_{GR}\rangle\right]^2\right) \\
G_R(\tau) &= \left(\langle C_R\rangle Diff_R + \langle C_{GR}\rangle Diff_{GR}\right) \Big/ \left(V_{eff}\left[\langle C_R\rangle + \langle C_{GR}\rangle\right]^2\right) \\
G^{\times}{}_{GR}(\tau) &= \langle C_{GR}\rangle Diff_{GR} \Big/ \left(V_{eff}\left[\langle C_G\rangle + \langle C_{GR}\rangle\right]\cdot\left[\langle C_R\rangle + \langle C_{GR}\rangle\right]\right)
\end{aligned}
\qquad (10)
$$

In the above equations the abbreviation $Diff_i$ describes the temporal evolution of the correlation curve for a single diffusing species *i*. C_G, C_R and C_{GR} are the time-dependent concentrations of the singly-labeled educts and the doubly-labeled product. It can easily be seen, that in the crosscorrelation curve (third expression of Eq. 10), the numerator contains only the signal from the reaction product bearing both dye labels, whereas the denominator is the product of sums of both labeled species containing

all the fluorescent molecules present in the system; this product is constant in time. Direct proportionality of the cross-correlation amplitude to the concentration of the reaction product is thus guaranteed. In contrast to the two autocorrelation curves, the temporal decay of the cross-correlation curve is exclusively governed by the diffusion characteristics of the product species, $Diff_{GR}$. This allows the dynamic behavior of the reaction product to be analyzed selectively.

4. Results of hybridization measurements by auto- and cross-correlation

4.1. Comparative single-color analysis of probe binding to RNA

Here we present two characteristic applications of the above concepts that have been carried out in our research group. In the first example [81] a comprehensive binding study has been carried out with six oligonucleotides, 17-37 basepairs long and labeled with tetramethylrhodamine; these probes bind to different sites of naturally folded 101 bp RNA targets. The experiments were based on the single-color method following Eq. 7. Association to the three to four times longer target resulted in a significant slowing down of the labeled probes. The idea behind this study was to compare the hybridization efficiencies of different probes to the different target regions; thereby, evidence for predicted secondary structure elements of the target RNA might be obtained. Formation of secondary structure via intramolecular hydrogen bonds always competes as a first order reaction with the second order hybridization processes; an intramolecular process is the more favored, the lower the concentrations are.

The measurements were carried out at a temperature of 40°C, this is above the melting temperatures of the probes, but below the calculated denaturation temperature of the target sequence (ca. 70°C). To guarantee temporal stability of the biochemical reaction system during FCS analysis, the measurements were performed in chemically inert open sample carriers. The concentrations used were 10 nM for the probes, and 10-50 nM for the target. Hybridization was followed by consecutive FCS measurements over 1 hour. Fig. 4 presents a representative example of the temporal evolution of the correlation curve in the time course of hybridization for one probe. Evaluation of the curves was simplified by careful calibration measurements of the diffusion times of the free and the bound probe τ_1 and τ_2. It turned out that the probe diffusion slowed down two- to threefold upon association.

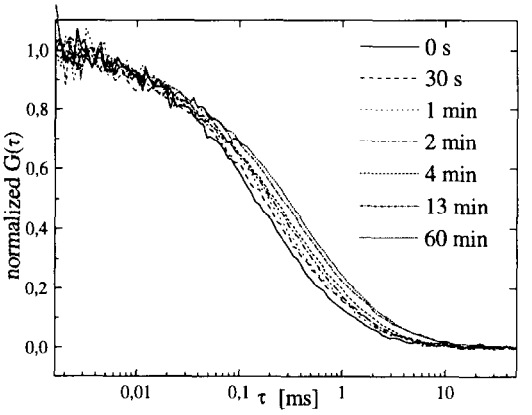

Fig. 4: Increase in correlation decay time during the time course of hybridization of a labeled probe (HS6) to the folded α-1 RNA target. The average diffusion time increases due to higher fractions of τ_2

To estimate the diffusion time of the complex before starting the hybridization process, an identical tetramethylrhodamine-labeled target RNA was hybridized to a 50 times excess of unlabeled probe. By knowing the diffusion time parameters τ_2 of the complexes and fixing them in the fitting routine, the product fractions Y could be obtained with a high confidence. The kinetics, Y plotted against incubation time of the hybridization, differ greatly from probe to probe (Fig. 5). However, it is obvious that although an excess of RNA was present, none of the probes was completely saturated within the observation time. After a rapid initial phase the kinetics slowed down significantly; this can be verified best in the case of probe HS6. Non-complete association was verified by employing a quantitated extension assay as an alternative method for measuring the extents of hybridization subsequent to the reaction. We showed that the curves in Fig. 5 could be described best by assuming a biphasic irreversible binding mechanism with a fast initial and a slow

second phase which could be due to inhomogeneities in the target's conformation.

The different probes exhibited initial rate constants in the range of 10^4 $M^{-1}s^{-1}$ to 10^6 $M^{-1}s^{-1}$. As expected, the largest rate constants were obtained for the probes which bind to the two open ends of the target sequence. The initial rates varied greatly due to the secondary structures and the accessibility of the target sites; this was found to be consistent with theoretically provided binding pathways [82,83].

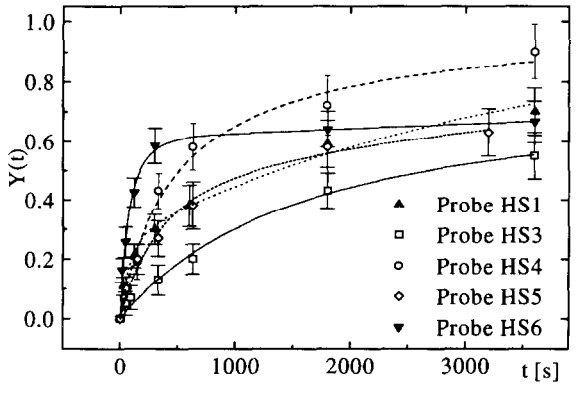

Fig. 5: Hybridization kinetics (fraction Y against time) of five different DNA oligonucleotide probes to the RNA target. Y is determined by evaluating the measurements (e.g. Fig. 4) with known τ_1, τ_2. The differences reflect the accessibility of binding sites at the folded target sequence.

4.2. *Cross-correlation performance*

The other approach for determining hybridization kinetics that we present here is a study of renaturation kinetics followed by dual-color cross-correlation [76]. In this measurement, the binding of two differently labeled complementary DNA oligonucleotides of the same length (40 b) was observed by following the change in the cross-correlation amplitude. The concentrations were 10nM for each probe. The fluorescent markers used for labeling of the probes, rhodamine green and Cy-5, are spectrally very well separated; their emission maxima are 520 nm and 670 nm respectively. The instrumentation setup in which the measurements were performed is shown in Fig. 6. For proper excitation of both dyes, two laser beams (488 nm line of argon-ion and 647 nm line of krypton-ion laser) simultaneously illuminate the microscope objective. By using a telescope system for adjusting the focal waist of at least one of the beams, it can be guaranteed that the illuminated focal volume, V_{eff} , is of the same size for both wavelengths. This is not a necessary condition for cross-correlation measurements, but considerably simplifies the evaluation of the obtained curves. Detection is performed by dividing the emission light into two channels after transmission of the pinhole by a dichroic mirror. Additional wavelength selectivity is provided by narrow bandpass filters in front of the detectors. Proper correction of the microscope objective against chromatic aberration is absolutely necessary for reliable performance of dual-color measurements. It is also critical to minimize the "spillover" of photons from the shorter wavelength dye into the "wrong" detector. Fig. 7 shows the increase in cross-correlation amplitude during the time course of hybridization reaction as well as the kinetic plot that can be obtained directly without a mathematical evaluation of the curves. By comparing Fig. 7 with Fig. 4, the differences between double- and single-color FCS hybridization reaction schemes can easily be visualized.

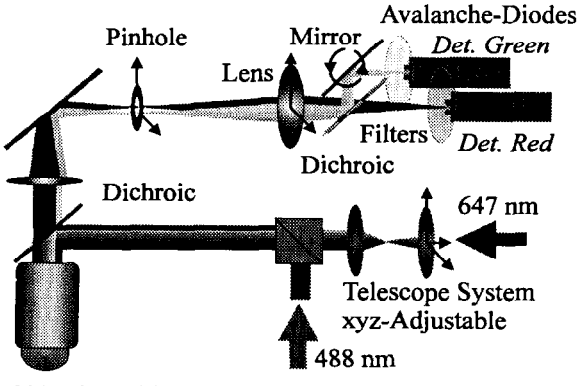

Fig. 6: Dual-color setup for cross-correlation measurements. The objective is epi-illuminated by two excitation laser beams. Using a telescope, identical focal spot size can be achieved. Emission light is divided by a dichroic mirror and detected by two avalanche diodes.

The only disadvantage of the crosscorrelation analysis in respect to the conventional single-color method is that the denominator of the cross-correlation curve contains the fluorescence from all

the species present in the system, which decreases the amplitude and lowers the statistical quality. This is apparent from the greater noise in.the curves in Fig. 7 compared to the curves in Fig. 4. It sets a lower limit for differentiating the doubly labeled fraction from singly labeled species, which can be estimated to be 1% in the present system.

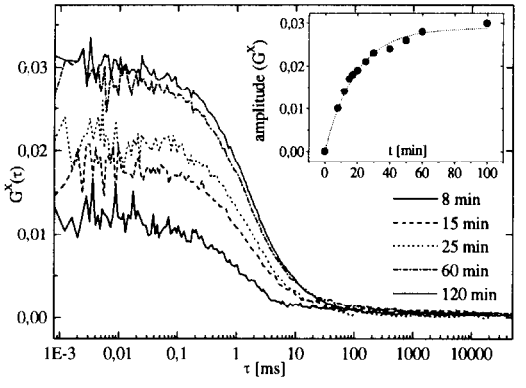

Fig. 7: Time course of cross-correlation analysis during the association of two differently labeled complementary DNA oligonucleotides. Kinetic data can be extracted by plotting the amplitude of the cross-correlation curve $G^X(\tau)$ against time. Assuming irreversible second-order reaction, we get an association constant of $k_{ass} = 8 \times 10^5\ M^{-1}s^{-1}$.

From our work we conclude that dual-color cross-correlation measurements of hybridization kinetics, although not as simple to perform as single-color diffusional analysis, is a very attractive alternative. This conclusion especially holds when no significant changes in diffusion constants occur, as is the case for two comparably short nucleic acids. For all kinetic investigations where reaction partners are of comparable molecular weights, such as a large variety of antigen-antibody or ligand-receptor interactions, we therefore advise the use of the dual-color cross-correlation method.

5. Diagnostic applications

Detection of minute amounts of pathogenic particles in an early state of infection is one of the most prominent and urgent problems in medical research. Although the ultimate goal of single-molecule detection strategies is to directly monitor the pathogenic nucleic acid material - viral or bacterial DNA or RNA - in blood plasma without the necessity of any amplification processes [39], considerable success has been obtained up to now by a rather pragmatic combination of amplification and FCS detection. The advantages of high-speed amplification are combined with the high detection sensitivity at an early state of the amplification process in order to construct an easy and highly specific test system with very low contamination, few artifacts and few false-negative samples. DNA as well as RNA amplification methods, PCR and 3SR, have been combined with FCS [80,84], the latter could be carried out conveniently by an isothermal reaction scheme (NASBA), which was then followed by on-line FCS-measurements. Initial HIV virus concentrations could be detected down to 10^{-18} M. A scheme for quantifying such low initial concentrations has been developed, which is based on the concentration dependence of the onset of FCS-specific changes in diffusion constants of the fluorescent molecules.

5.1. *Diagnosis of HIV infection*

Normally, in the first stage of infection a burst of viremia is observed, which is then drastically reduced by the immune response [85]. An equilibrium between the host and the virus follows this initial reaction; this state is maintained for years and differs from individual to individual. The steady-state level is highly predictive of the long-term clinical outcome [86]. Therefore, new studies have focused on measuring HIV-1 RNA in cells and especially in blood plasma for predicting the disease progression [87]. The results of these studies clearly indicate a poorer prognosis for subjects with persistently high viral loads in the plasma [88]. Not only is it important to determine the number of HIV-1 RNA molecules in plasma for the prediction of the AIDS disease progression, but this number also directly reflects the success and efficiency of an antiviral therapy. O'Brien *et al.* [89] have demonstrated that the reduction of the viral load in blood is a direct response to zidovudine therapy. When applying a combination treatment with indinavir, zidovudine and lamivudine, the viral load was reduced to less than 1%; in 85% of

the infected individuals plasma viremia had become undetectable after 24 weeks of treatment.

Many methods for the quantitation of HIV-1 RNA have been developed in the last few years: RNA-PCR [90], NASBA [91] self-sustained sequence replication reaction (3SR) [92,93], transcription-based amplification system (TAS) [94] and branched-DNA signal amplification assay [95]. HIV-1 RNA concentrations in plasma normally range from less than 500 to 300,000 molecules/ml when quantified with a branched-DNA signal amplification assay (quantitation limit of this assay: 500 molecules/ml plasma), which is the most sensitive method available at the moment [96].

5.2. *Nucleic acid sequence-based amplification combined with FCS*

The nucleic acid sequence-based amplification (NASBA) method that we focus on, has a detection threshold of 1000 HIV-1 RNA molecules per ml blood plasma [97]. In contrast to PCR-based methods, NASBA is a cyclic isothermal amplification reaction where a specific part of an RNA target molecule is amplified first by reverse transcription and subsequently by transcription of the DNA by T7 RNA polymerase. Quantitation of the initial RNA concentration by NASBA is achieved by a one-tube reaction using three distinguishable internal RNA standards at different concentrations (Q_A 10^4, Q_B 10^3, Q_C 10^2 molecules); these are amplified together with the unknown HIV-1 wild-type RNA sample. The wild-type RNA and the three standards are detected separately with probes labeled by electrochemiluminescence (ECL). The amount of initial RNA can be calculated from the ratio of wild-type RNA signal to Q_A, Q_B and Q_C signals [98]. Since the use of three internal standards for the ECL quantitation of target RNA is a relatively demanding procedure, FCS technology was combined with the NASBA system [84]. Coupling of NASBA with FCS detection is possible by introducing a fluorescently labeled DNA probe into the amplification reaction, which hybridizes to a distinct position of the amplified RNA molecule. The extension of this probe during NASBA is monitored *online* by measuring the increase of its diffusion time by FCS. In order to simulate HIV-1 infection, one milliliter of human blood plasma was spiked with different concentrations of genomic HIV-1 RNA [99]. After a lysis step and re-isolation of the HIV-1 target RNA, the NASBA reaction was carried out in the presence of the labeled DNA probe [97].

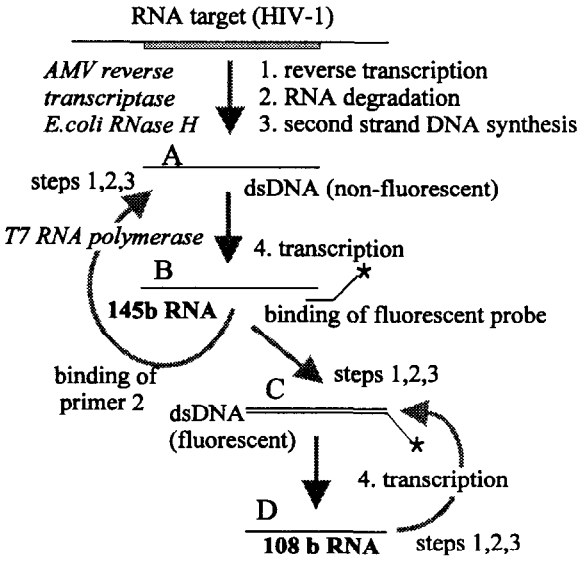

Fig. 8: NASBA reaction scheme of HIV-1 RNA. In the initial non-cyclic phase, a 145b stretch of the RNA target is reverse transcribed into ds DNA (A). Subsequent transcription results in the formation of RNA molecules (B). B is now subjected to the cyclic phase of NASBA: Binding of primer 2 yields again product A, whereas binding of the fluorescent probe yields DNA species C. C is then processed to a 108b RNA molecule (D). The formation of D is monitored *online* by FCS.

The influence of this probe on the reaction mechanism is demonstrated in Fig. 8: The amplification starts with binding of primer 1 (comprising the T7 promoter sequence) to a specific sequence of the *gag* region, which initiates reverse transcription by avian myeloblastosis virus reverse transcriptase (AMV RT). After degradation of the RNA in the resulting DNA-RNA hybrid by *E. coli* RNase H, second-strand DNA synthesis (triggered by primer 2 binding) takes place. The dsDNA is transcribed into RNA by T7 RNA polymerase yielding antisense RNA molecules with the length of 145 bases. Since the ratio between the amplification primers 1 and 2 and the labeled DNA probe is about 50:1, the 145 b RNA molecule is the predominant product of the first

(non-cyclic) phase of NASBA. In the following cyclic phase either "normal" 145 b RNA or 108 b RNA (resulting from probe binding to the antisense RNA molecule) is synthesized. The rate of hybridization and extension of the labeled DNA probe is proportional to the formation rate of the RNA amplification products. This is the crucial point in combining NASBA with FCS detection: Its diffusion time and, therefore, its extension rate can be measured *online* in FCS by the provided diffusional analysis.

5.3. Results

The experiments were performed in a special plastic foil containing 96 wells. The wells were filled with the NASBA reaction mixture, sealed, fixed in a thermoblock (pre-thermostatted at 42°C) and set under the objective (Fig. 9). The laser is focused into the samples through the walls of the plastic foil. After the measurements, the foils were discarded without opening - the contamination risk is therefore drastically reduced.

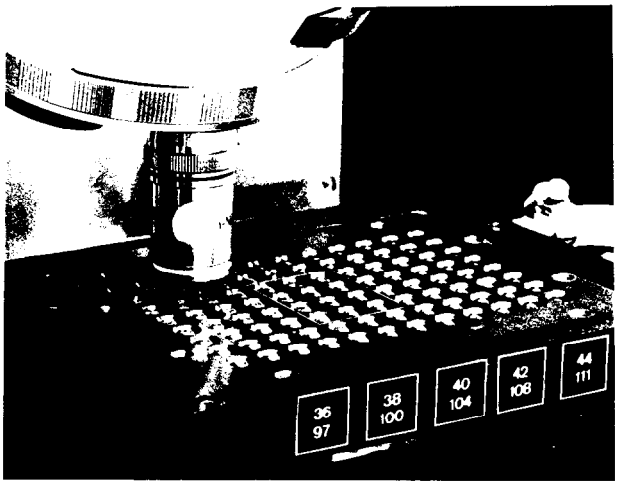

Fig. 9: Thermoblock (42°C) with 96 sealed plastic wells for *online* detection of the NASBA reaction. The wells are shaped as hemispheres, the detection is performed from above through the convexity.

During the NASBA reaction a shift of the autocorrelation curve towards tonger decay times, due to the elongation of the probe, is observed. The results are compared with a sample where no infectious agent was added (Fig. 10). In order to determine the exact rate of extending the probe during the course of NASBA, the autocorrelation curves had to be evaluated quantitatively. Knowing the diffusion time of the free probe, the autocorrelation curves were fitted with Eq. 7, yielding the fraction of elongated probe in dependence of NASBA incubation time (Fig. 11). The initial phase of these extension kinetic curves can be described by a single exponential function: $P(t) = P_0 \exp(kt)$. The rate constant k reflects the NASBA mechanism and P_0 the initial number of RNA template molecules in the blood sample.

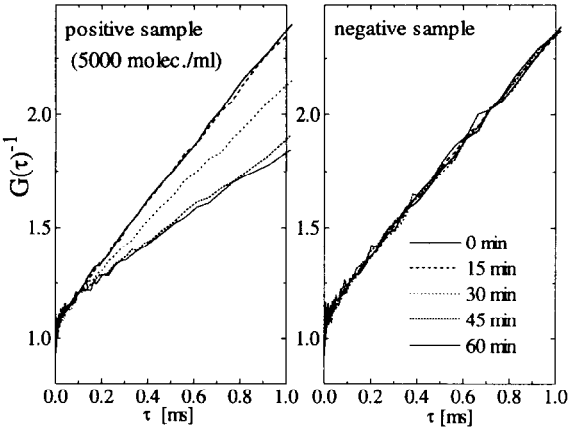

Fig. 10: Test for HIV-1 infection by NASBA-FCS. The correlation curves are plotted in reciprocal manner. Due to probe binding and elongation in the positive sample, the average diffusion time increases significantly during the amplification process. No effect is observed in the negative sample.

The quantitation of RNA in blood plasma by NASBA-FCS should not be restricted to the diagnostic sector. Another interesting field may be the investigation of gene activity by quantifying the corresponding mRNA, because gene expression is regulated at the level of DNA transcription into mRNA. High-throughput screening of the activity of many different genes in parallel may become one of the most important future applications.

6. Conclusion

FCS has developed far beyond the experimental stage to become a reliable method for studying kinetic processes in minute samples. In the autocorre-

lation mode it is most suitable for reactions that take place in the time range of minutes to hours, and where the diffusion constants of the reaction partners change. Measurements of nucleic acid hybridization kinetics as well as other applications have demonstrated the power of the method. New concepts in FCS such as the dual-color cross-correlation method overcome the requirement of marked diffusional changes. This greatly increases the number of applications accessible to FCS measurements and allows definite decisions to be made whether a binding reaction has occurred. The possibility for detecting and characterizing minute amounts of target molecules, e.g. viral RNA, in a large background of unspecific molecules marks the potential of FCS for diagnostic purposes.

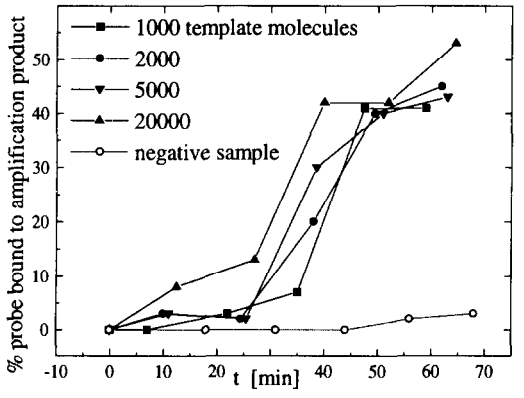

Fig. 11: Fraction of bound and/or elongated probe during the NASBA amplification process, given by evaluation of the curves Fig. 10. The more HIV-1 RNA molecules are infected, the earlier a significant shift in the correlation decay time occurs. This opens up the possibility for quantitation schemes.

The combination of NASBA amplification with FCS detection proved to be a feasible and sensitive method for the quantitative detection of HIV-RNA. Beyond the quantitation of nucleic acids, FCS opens up the possibility for sensitively monitoring aggregation processes. The use of FCS for diagnosing illnesses that are characterized by aggregation, such as prion diseases, may also prove to be an important future application [100].

Acknowledgements

We want to thank Prof. Manfred Eigen for his support and advice, for valuable discussions, proposals for experiments and data evaluation (reciprocal plot). Further, we thank Prof. Rudolf Rigler, KI Stockholm, for help and advice in constructing the confocal FCS setup and for his fruitful collaboration with our department. This work was financially supported by Grant No. 0310739 from the German Ministry for Education and Research, and by EVOTEC BioSystems GmbH, Hamburg.

References

[1] L. Onsager, Phys. Rev. 37 (1931) 405.
[2] N. O. Petersen and E.L. Elson, Methods Enzymol. 130 (1986) 454.
[3] E.L. Elson and W.W. Webb, Ann. Rev. Biophys. Bioeng. 4 (1975) 311.
[4] T. Svedberg, Z. Phys. Chem. 77 (1911) 147.
[5] M. v. Smoluchowski, Wien Berichte 123 (1914) 2381.
[6] B. J. Berne and R. Pecora, Dynamic light scattering, with applications to chemistry, biology, and physics (Wiley, New York, 1975)
[7] D. Magde, E.L. Elson, and W.W. Webb, Phys. Rev. Lett. 29 (1972) 705.
[8] E.L. Elson and D. Magde, Biopolymers 13 (1974) 1.
[9] M. Ehrenberg and R. Rigler, Chem. Phys. 64 (1974) 390.
[10] D. Magde, E.L. Elson, and W.W. Webb, Biopolymers 13 (1974) 29.
[11] S.R. Aragon and R. Pecora, Biopolymers 14 (1975) 119.
[12] S.R. Aragon and R. Pecora, J. Chem. Phys. 64 (1976) 1791.
[13] H. Weissman, H. Schindler, and G. Feher, Proc. Natl. Acad. Sci. USA 73 (1976) 2776.
[14] T. Meyer and H. Schindler, Biophys. J. 54 (1988) 983.
[15] A.G. Palmer and N.L. Thompson, Chem. & Phys. Lipids 50 (1989) 253.
[16] J.R. Abney, B.A. Scalettar, and C.R. Hackenbrock, Biophys. J. 58 (1990) 261.
[17] H. Qian and E.L. Elson, Biophys. J. 57 (1990) 375.
[18] A.G. Palmer and N.L. Thompson, Biophys. J. 52 (1987) 257.
[19] N.O. Petersen, Biophys. J. 49 (1986) 809.
[20] N.O. Petersen, D.C. Johnson, and M.J. Schlesinger, Biophys. J. 49 (1986) 817.
[21] P.R. St-Pierre and N.O. Petersen, Biophys. J. 58 (1990) 503.
[22] D.E. Koppel, F. Morgan, A.E. Cowan, and J.H. Carson, Biophys. J. 66 (1994) 502.

[23] Z. Huang and N.L. Thompson, Biophys. J. 70 (1996) 2001.
[24] D.E. Koppel, D. Axelrod, J. Schlessinger, E.L. Elson, and W.W. Webb, Biophys. J. 16 (1976) 1315.
[25] P.F. Fahey, D.E. Koppel, L.S. Baraks, D.E. Wolf, E.L. Elson, and W.W. Webb, Science 195 (1977) 305.
[26] J. Borjedo, Biopolymers 18 (1979) 2807.
[27] R. Rigler, P. Grasseli, and M. Ehrenberg, Physica Scripta 19 (1979) 468.
[28] P. Kask, P. Piksarv, Ü. Mets, M. Pooga, and E. Lippmaa, Eur. Biophys. J. 14 (1987) 257.
[29] D. Magde, W.W. Webb, and E.L. Elson, Biopolymers 17 (1978) 361.
[30] H. Asai, Jap. J. Appl. Phys. 19 (1980) 2279.
[31] J. Ricka and T. Binkert, Phys. Rev. A 39 (1989) 2646.
[32] K.Q. Xia, Y.B. Xin, and P. Tong, J. Opt. Soc. Am. A 12 (1995) 1571.
[33] M. Brinkmeier and R. Rigler, Exp. Techn. Phys. 41 (1995) 205.
[34] R. Rigler and J. Widengren, Bioscience 3 (1990) 180.
[35] R. Rigler, Ü. Mets, and J. Widengren, in: Fluorescence Spectroscopy, ed. O.S. Wolfbeis (Springer, Berlin, 1992), p. 13.
[36] R. Rigler and Ü. Mets, Soc. Photo-Opt. Instrum. Eng. 1921 (1992) 239.
[37] J. Widengren, R. Rigler, and Ü. Mets, J. Fluoresc. 4 (1994) 255.
[38] J. Widengren, Ü. Mets, and R. Rigler, J. Chem. Phys. 99 (1995) 13368.
[39] M. Eigen and R. Rigler, Proc. Natl. Acad. Sci. USA 91 (1994) 5740.
[40] M. Eigen, Angew. Chemie 80 (1968) 892.
[41] C.F. Bernasconi, Investigation of rates and mechanisms of reactions, Part II, 4th ed. (Wiley, New York 1986).
[42] M. Eigen, Naturwissenschaften 58 (1971) 465.
[43] M. Eigen, Gene 135 (1993) 37.
[44] D. Gillespie, S. Spiegelman, J. Mol. Biol. 12 (1965) 829.
[45] R.J. Britten, D.E. Kohne, Science 161 (1968) 529.
[46] M.L.M. Anderson, B.D. Young in: Nucleic Acids Hybridization: A Practical Approach, eds. B.D. Hames, S.J. Higgins (IRL Press Oxford 1985) pp 73-102.
[47] J.G. Wetmur, Critical Reviews in Biochemistry & Molecular Biology 26 (1991) 227.
[48] J. Boni, J. Schupbach , Molecular & Cellular Probes 7 (1993) 361.
[49] H.J. Watts, D. Yeung, H. Parkes, Anal. Chem. 67 (1995) 4283.
[50] R.J. Britten, D.E. Graham, B.R. Neufeld in: Methods in Enzymology, eds. L. Grossman, K. Moldave, Vol 29 (Academic Press, London 1974) pp. 363-418
[51] J.O. Bishop, J.G. Morton, M. Richardson, Nature 250 (1974) 199.
[52] P.P. Zarrinkar, J.R. Williamson, Science 265 (1994) 918.
[53] Y. Kumazawa, T. Yokogawa, H. Tsurui, K. Miura, K. Watanabe, Nucleic Acids Res. 20 (1992) 2223.
[54] M.K. Dewanjee, A.K. Ghafouripour, M. Kapadvanjwala, A.T. Samy, Biotechniques 16 (1994) 844.
[55] B.L. Karger, F. Foret, J. Berka, Methods in Enzymology 271 (1996) 293.
[56] D.J. Rose, Anal. Chem. 65 (1993) 3545.
[57] U. Vincent, H. Patra, J. Therasse, P. Gareil, Electrophoresis 17 (1996) 512.
[58] D.L. Deforce, F.P. Ryniers, E.G. van den Eeckhout, F. Lemiere, E.L. Esmans, Anal. Chem. 68 (1996) 3575.
[59] C.A. Bush in: Basic Principles in Nucleic Acids Chemistry, ed. P.O.P. Ts'O, Vol 2 (Academic Press, New York 1974) pp 91-169
[60] D. Pörschke, M. Eigen, J. Mol. Biol. 62 (1971) 361.
[61] K.J. Breslauer in: Thermodynamic Data for Biochemistry, ed. H.-J. Hinz (Springer, New York 1986) pp. 402-27.
[62] D.J. Patel, A. Pardi, K. Itakura, Science 216 (1982) 581.
[63] Y. Li, P.C. Bevilacqua, D.Mathews, D.H. Turner, Biochemistry 34 (1995) 14394.
[64] S. Tyagi, F.R. Kramer, Nature Biotechnol. 14 (1996) 303.
[65] K.M. Parkhurst and L.J. Parkhurst, Biochemistry 34 (1995) 285.
[66] T.A. Perkins, D.E. Wolf, J. Goodchild, Biochemistry 36 (1996) 16370.
[67] S.M. Sorscher, J.C. Bartholomew, and M.P. Klein, Biochim. Biophys. Acta 610 (1980) 28.
[68] R.D. Icenogle and E.L. Elson, Biopolymers 22 (1983) 1919, 1949.
[69] N.L. Thompson and D. Axelrod, Biophys. J. 43 (1983) 103.
[70] M. Kinjo and R. Rigler, Nucleic Acids Res. 23 (1995) 1795.
[71] B. Rauer, E. Neumann, J. Widengren, R. Rigler, Biophys. Chem. 58 (1996) 3.
[72] S. Sterrer and K. Henco, J. Receptor & Signal Transd. Res. 17 (1997) 511.
[73] R. Rigler, Ü. Mets, J. Widengren, and P. Kask, Eur. Biophys. J. 22 (1993) 169.
[74] D.E. Koppel, Phys. Rev. A. 10 (1974) 1938.
[75] Ü. Mets and R. Rigler, J. Fluoresc. 4 (1994) 259.
[76] P. Schwille, F.J Meyer-Almes, and R. Rigler, Biophys. J. 72 (1997) 1878.
[77] N.L.Thompson, in: Topics in Fluorescence Spectroscopy, ed. J.R. Lakowicz, Vol. 1 (Plenum Press, New York 1991) 337.
[78] M. v. Smoluchowski, Physik. Z. 17 (1916) 557.
[79] H. Qian and E.L. Elson, Appl. Opt. 30 (1991) 1185.
[80] N.G. Walter, P. Schwille, and M. Eigen, Proc. Natl. Acad. Sci. USA 93 (1996) 12805.
[81] P. Schwille, F. Oehlenschläger, and N.G. Walter, Biochemistry 35 (1996) 10182.
[82] E.G.H. Wagner and R.W. Simons, Annu. Rev. Microbiol. 48 (1994) 713.
[83] T.A.H. Hjalt and E.G.H. Wagner, Nucleic Acids Res.

23 (1995) 580.
[84] F. Oehlenschläger, P. Schwille, M. Eigen, Proc. Natl. Acad. Sci. USA 93 (1996) 12811.
[85] G. Pantaleo, J.F. Demarest, H. Soudeyns, C. Graziosi, F. Denis, J.W. Adelsberger, P. Borrow, M.S. Saag, G.M. Shaw, R.P. Sekaly et al, Nature 370 (1994) 463.
[86] J.W. Mellors, C.R. Rinaldo Jr.,P. Gupta, R.M. White, J.A. Todd, L.A. Kingsley, Science 272 (1996) 1167.
[87] D.H. Ho, Science 272 (1996) 1124.
[88] K. Saksela, C.E. Stevens, P. Rubinstein, P.E. Taylor, D. Baltimore, Ann. Intern. Med. 123 (1995) 641.
[89] W.A. O'Brien, P.M. Hartigan, D. Martin, J. Esinhart, A. Hill, S. Benoit, M. Rubin, M.S. Simberkoff, J.D. Hamilton, N. Engl. J. Med. 334 (1996) 426.
[90] S. Escaich, J. Ritter, Ph. Rougier, D. Lepot, J.-P. Lamelin, M. Sepetjan, Ch. Trepo, AIDS 5 (1991) 1189.
[91] J. Compton, Nature 350 (1991) 91
[92] J.C. Guatelli, K.M. Whitfield, D.Y. Kwoh, K.J. Barringer, D.D. Richman,T.R. Gingeras, Proc. Natl. Acad. Sci. USA 87 (1990) 1874.
[93] M. Gebinoga, F. Oehlenschläger, Eur. J. Biochem. 235 (1996) 256.
[94] D.Y. Kwoh, G.R. Davis, K.M. Whitfield,H.L. Chapelle, L.J. DiMichele, T.R. Gingeras, Proc. Natl. Acad. Sci. USA 86 (1989) 1173.
[95] M.S. Urdea, Clin. Chem. 39 (1993) 725.
[96] J. Todd, C. Pachl, R. White, T. Yeghiazarian, P. Johnson,B. Taylor, M. Holodniy, D. Kern, S. Hamren, D. Chernoff et al., J. AIDS Human Retrovir. 10 (1995) 35.
[97] B. van Gemen, T. Kievits, R. Schukkink, D. van Strijp, L.T. Malek, R. Sooknanan, H.G. Huisman, P. Lens, J. Virol. Meth. 43 (1993) 177.
[98] B. van Gemen, R. van Beuningen, A. Nabbe, D. van Strijp, S. Jurriaans, P. Lens, T. Kievits, J. Virol. Methods 19 (1994) 157.
[99] L. Ratner, W. Haseltine, R. Patarca, K.J. Lavak, B. Starich et al., Nature 313 (1985) 277.
[100] M. Eigen, Biophys. Chem. 63 (1996) A1.